A COMMUTATOR WITH INTEGRATED CAPACITORS

[1]Boris Benedičič, [2]France Pavlovčič, [3]Janez Nastran, [1]Jožica Rejec

[1]R&D Department, Domel d.d., Železniki, Slovenia
[2]Environmental Agency of the Republic of Slovenia, Ministry of environment, spatial planning and energy, Ljubljana, Slovenia
[3]University in Ljubljana, Faculty for Electrical Engineering, Ljubljana, Slovenia

Key words: commutation, universal motor, capacitor, finite element method, arc model.

Abstract: The paper presents a method of an improvement of commutation of a high-speed universal commutator motor with ceramic capacitors integrated in a commutator. A model of the motor was established to enable an analysis of an armature coil commutation. The capacitors were included in the model as well. A prototype motor with integrated capacitors was made. The multilayer ceramic capacitors in the form of surface mounted chips were used. Good (sparkless) commutation is essential for long operational lifetime of the commutator motor. The calculation of internal brush resistances and non-linear coil inductances was made with the finite element method . Brush contact resistances were also calculated. All resistances and inductances were calculated with respect to the rotor position. An actual overlap between the brush and the commutator segment was taken into consideration. A suitable arc model was used to estimate the arc, which varies with the width of the charred layer on the brush. The calculated results are compared with the ones measured on a special test motor. It was found out from calculation and from the measurement which closely agree, that the rightly chosen capacitors greatly improve the commutation of the motor and therefore extend the lifetime of the motor significantly.

Komutator z integriranimi kondenzatorji

Kjučne besede: komutacija, univerzalni motor, kondenzator, metoda končnih elementov, model obloka.

Izvleček: V prispevku predstavljamo izboljšavo komutacije hitrotekočega univerzalnega motorja z kondenzatorji, integriranimi v komutator. Izdelali smo računalniški model komutacije, ki omogoča analizo komutacijskih tokov v posameznih rotorskih tuljavah. Kondenzatorji so bili prav tako vključeni v model. Izdelali smo tudi prototipe motorjev z integriranimi kondenzatorji. Uporabljeni so bili večplastni keramični kondenzatorji izdelani v SMD tehnologiji. Dobra komutacija brez oblokov je bistvena za dolgo življenjsko dobo komutatorskih motorjev. Za določitev porazdeljenih upornosti ščetk in induktivnosti tuljav v računalniškem modelu smo uporabili metodo končnih elementov. Upornosti so bile odvisne od relativnega položaja komutator - ščetka, prav tako tudi induktivnosti, ki so bile odvisne še od toka, ki je tekel skoznje. Upoštevali smo realno prekrivanje ščetka - komutatorska lamela, to je 1,8. Zaradi takega prekrivanja smo morali upoštevati, da dve tuljavi komutirata istočasno. Izračunali smo tudi kontaktne upornosti. Za upoštevanje nastanka obloka smo uporabili model po Holmu /9/, ki določa pogoje za nastanek obloka v odvisnosti od kontaktnih materialov. Ugotovili smo, da pojav obloka pod ščetko povzroči spremembe na ščetki, kjer nastane ožgana plast, ki ima slabšo prevodnost od ščetke same. Nastanek te plasti močno vpliva na potek komutacijskih tokov. Izračunane komutacijske tokove smo primerjali s tokovi, izmerjenimi na prirejenem motorju, ki je imel konce dveh rotorskih tuljav izvedene na drsne obroče. Izračunani rezultati so se dovolj dobro približali merjenim rezultatom. Komutacija se tako pri izračuni kot pri meritvi zelo izboljša, če v komutacijski krog vključimo kondenzatorje. Podali smo kriterije za pravilno izbiro kondenzatorjev, ki najbolj učinkovito izboljšajo potek komutacije. Zaradi izboljšane komutacije s kondenzatorji se podaljša tudi življenjska doba motorja.

1. Introduction

The universal motor is one of the most common motors used in domestic appliances. It is a commutator motor that has its field winding connected in series with the armature winding. The revolving speed of this motor is increasing because of the tendency to decrease both the motor size and weight. It is not uncommon for this motor to have 50000 rpm or more. But good commutation (current direction change) is difficult to achieve at such high speeds.

The commutation in the commutating armature coil has to be fast enough to enable minimizing the current difference at the moment, when the commutator bar is leaving the brush. Excessive current differences give rise to the development of sparks and arcs, which shortens the motor operational lifetime through an increased brush wear. Moreover, the arc may occur before the commutator bar leaves the brush, if a voltage between the brush and the bar is large enough. The aim of this paper is to present a method of improvement of commutation with capacitors integrated in the commutator of the motor. The capacitors absorb the inductive energy which would otherwise disperse in the arcs and therefore greatly improve the commutation.

Until recently, the commutation phenomena has been mainly investigated on DC machines, preferably equipped with interpole windings /1,2/, which significantly improve the commutation. The commutation in AC universal motors is much worse compared to the one in the DC motors. One of the causes for this state is the absence of interpoles and the other is the presence of transformer EMF because of the AC line voltage. Authors in /3/ researched the universal motor commutation, where during one commutation period constant current is presumed. For the calculation of the circuit parameters (inductances and flux linkages) they used the finite element method. In /4/ the universal motor model is improved by using the real current and by modelling brush resistances with the finite element method, though the arc model is somehow simplified.

The model of the commutator motor with the integrated capacitors is presented, with which the commutation current and other commutation related phenomena in small universal motor can be analysed. The inductances, the flux linkages and the brush resistances for the model are calculated with the finite element method. The commutation equation is solved iteratively until the calculated currents converge. The arc model is improved by using the arc U/I characteristics /6/. The change in the contact resistance and the appearance of the charred layer on the brush due to the arc under the brush are explained. With this model, the optimal value of capacitance of integrated capacitors was calculated to diminish the arc. These capacitors were mounted on a special prototype motor with slip rings. The improvement of commutation both in the computer model and in the prototype motor was found to be satisfactory and the lifetime of the motor was extended.

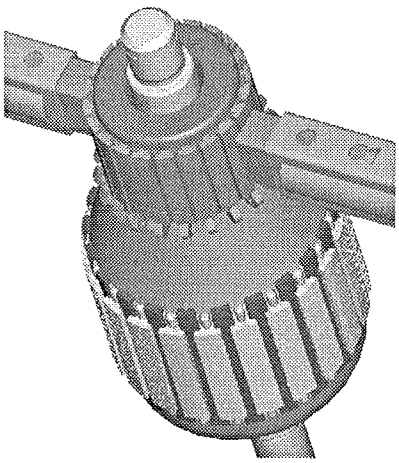

Figure 1: A universal motor rotor and brushes.

2. A universal motor circuit topology and model equations

The circuit topology of the two-pole universal motor is shown in Fig. 2. Because the brush-to-bar width ratio is 1.8, there are two possibilities: in the first one the brush covers two commutator bars and in the second one the brush covers three bars. In our model, both topologies are used, with a proper transition from one topology to the other, depending on the brush - bar position.

The circuit in Fig. 2 is symmetrical, so it can be simplified. Four commutating coils in Fig. 2 are considered as two paralleled windings. The parallel rotor winding branches in series with the field winding are replaced with one equivalent winding. Consequently, when the brush covers three commutator bars, there are three windings in the system - two commutation windings and one main winding. But, if the brush covers only two bars, there are two windings, the commutation one and the main one in the system.

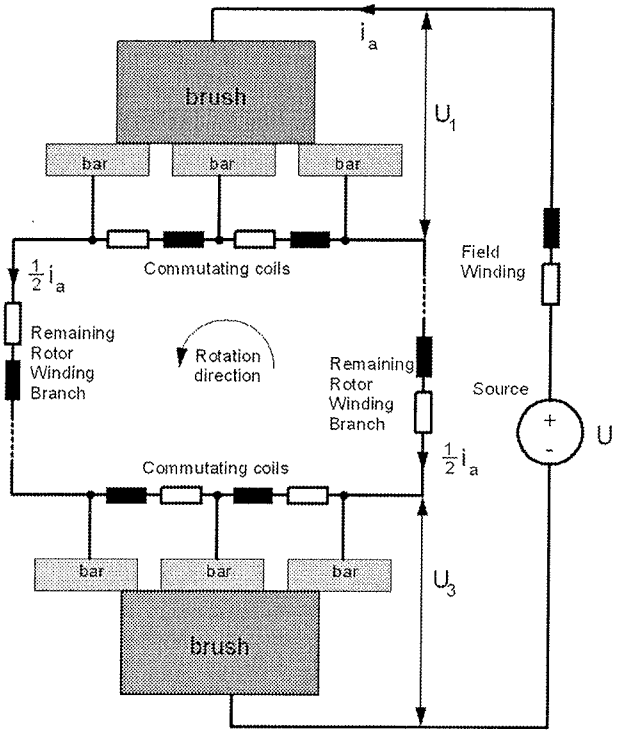

Figure 2: The universal motor circuit topology - the brush covers three bars.

The capacitors are connected parallel to the commutating windings. In series with the capacitor there is the damping resistance R_c. Fig. 3 shows two parallel commutating windings (L_{33}, R_3 and L_{44}, R_4), the capacitor C and the damping resistance R_c. The contact resistances R_{c1}, R_{c2} and R_{c3} can also be observed.

The main Equation (1) for Fig. 2 is:

$$U = (R_1 + R_2) \cdot i_a + \frac{d\psi_a}{dt} + U_1 + U_3 \qquad (1),$$

where:

U is the applied voltage,
R_1 is the field winding resistance,
R_2 is the resistance of the non-commutating parallel armature winding branches,
i_a is the main current,
ψ_a is the total flux linkage of the main winding,
U_1, U_2 and U_3 are the commutator bar voltages.

From Fig. 3 the following voltage Eqs. (2,3), are derived:

$$U_1 - U_2 = R_3 \cdot i_{c3} + \frac{d\psi_3}{dt} \qquad (2),$$

$$U_2 - U_3 = R_4 \cdot i_{c4} + \frac{d\psi_4}{dt} \qquad (3),$$

where:

ψ_3, ψ_4 are the total flux linkage commutating windings,
R_3, R_4 are the commutating winding resistances,
i_{c3}, i_{c4} are the commutating currents.

For the capacitor branch from Fig. 3 Eqs. (4,5) can be written:

$$U_1 - U_2 = R_c \cdot i_{cc1} + \frac{1}{C} \cdot \int i_{cc1} dt \quad (4),$$

$$U_2 - U_3 = R_c \cdot i_{cc2} + \frac{1}{C} \cdot \int i_{cc2} dt \quad (5),$$

where:

C is the capacitance of the integrated capacitor,
R_c is the damping resistance,
i_{cc1}, i_{cc2} are the capacitor currents.

The connection between the commutator bar voltages and the currents is defined by Eq. (6):

$$\begin{bmatrix} U_1 \\ U_2 \\ U_3 \end{bmatrix} = \begin{bmatrix} r_{11} + r_{c1} & r_{12} & r_{13} \\ r_{12} & r_{22} + r_{c2} & r_{23} \\ r_{13} & r_{23} & r_{33} + r_{c3} \end{bmatrix} \cdot \begin{bmatrix} i_1 \\ i_2 \\ i_3 \end{bmatrix} \quad (6),$$

where:

r_{11}, r_{12}, r_{13}, r_{22}, r_{23}, r_{33} are elements of the brush resistance matrix,
r_{c1}, r_{c2}, r_{c2} are the brush contact resistances,
i_1, i_2, i_3 are commutator bar currents.

The value of the above resistances depends on the instantaneous brush position with respect to the commutator bars. The brush resistance matrix elements are determined by the brush dimensions and the brush material properties (e.g. material specific resistances).

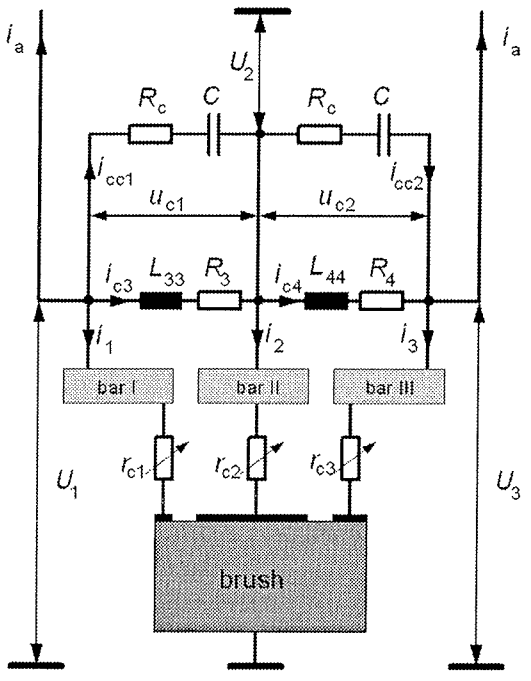

Figure 3: The brush with the parallel commutating windings and the integrated capacitors.

According to Fig. 3, the commutator bar currents are defined as:

$$i_1 = -i_a - i_{c3} - i_{cc1} \quad (7),$$

$$i_2 = i_{c3} - i_{c4} + i_{cc1} - i_{cc2} \quad (8),$$

$$i_3 = -i_a + i_{c4} + i_{cc2} \quad (9).$$

Energy in the capacitors is represented by the capacitor voltage. The capacitor voltages are defined in (10) and (11):

$$U_1 - U_2 = u_{c1} \quad (10),$$

$$U_2 - U_3 = u_{c2} \quad (11).$$

When the matrix (6) with the currents (7), (8), (9) is inserted in Eqs. (10) and (11) the following two equations for the capacitor voltage are obtained - (12) and (13):

$$\begin{aligned} u_{c1} &= -i_a \cdot R_{21} - i_{c3} \cdot (R_{22} - R_3) - \\ & i_{c4} \cdot R_{23} - i_{cc1} \cdot (R_{22} - R_3) - i_{cc2} \cdot R_{23} \end{aligned} \quad (12),$$

$$\begin{aligned} u_{c2} &= -i_a \cdot R_{31} - i_{c3} \cdot R_{32} - i_{c4} \cdot (R_{33} - R_4) \\ & - i_{cc1} \cdot R_{32} - i_{cc2} \cdot (R_{33} - R_4) \end{aligned} \quad (13),$$

The resistances in the above equations are (14):

$$\begin{aligned} R_{21} &= r_{11} + r_{c1} + r_{13} - r_{12} - r_{23} \\ R_{22} &= R_3 + r_{11} + r_{c1} - 2r_{12} + r_{22} + r_{c2} \\ R_{23} &= r_{12} - r_{13} - r_{22} - r_{c2} + r_{23} \\ R_{31} &= r_{12} - r_{13} + r_{23} - r_{33} - r_{c3} \\ R_{32} &= r_{12} - r_{13} - r_{22} - r_{c2} + r_{23} \\ R_{33} &= R_4 + r_{22} + r_{c2} - 2r_{23} + r_{33} + r_{c3} \end{aligned} \quad (14).$$

From the equations (12) and (13), the equations of the capacitor currents are derived - (15) and (16):

$$i_{cc1} = -u_{c1} \cdot g_{11} + u_{c2} \cdot g_{12} + i_a \cdot k_1 - i_{c3} \quad (15),$$

$$i_{cc2} = u_{c1} \cdot g_{21} - u_{c2} \cdot g_{22} + i_a \cdot k_2 - i_{c4} \quad (16).$$

Where the conductances $g_{11}...g_{22}$ and the coefficients k_1 and k_2 are:

$$\begin{aligned} g_{11} &= \frac{R_{33} - R_4}{(R_{22} - R_3) \cdot (R_{33} - R_4) - R_{23} \cdot R_{32}} \\ g_{12} &= \frac{R_{23}}{(R_{22} - R_3) \cdot (R_{33} - R_4) - R_{23} \cdot R_{32}} \\ g_{21} &= \frac{R_{32}}{(R_{22} - R_3) \cdot (R_{33} - R_4) - R_{23} \cdot R_{32}} \\ g_{22} &= \frac{R_{22} - R_3}{(R_{22} - R_3) \cdot (R_{33} - R_4) - R_{23} \cdot R_{32}} \\ k_1 &= \frac{R_{31} \cdot R_{23} - R_{21} \cdot (R_{33} - R_4)}{(R_{22} - R_3) \cdot (R_{33} - R_4) - R_{23} \cdot R_{32}} \\ k_2 &= \frac{R_{21} \cdot R_{32} - R_{31} \cdot (R_{22} - R_3)}{(R_{22} - R_3) \cdot (R_{33} - R_4) - R_{23} \cdot R_{32}} \end{aligned} \quad (17).$$

The time derivative of the capacitor voltages are obtained by inserting Eqs. (15) and (16) into Eqs. (4) and (5), and are represented by Eqs. (18) and (19):

$$\frac{du_{c1}}{dt} = R_c \cdot \left(-\frac{du_{c1}}{dt} \cdot g_{11} + \frac{du_{c2}}{dt} \cdot g_{12} + \frac{di_a}{dt} \cdot k_1 - \frac{di_{c3}}{dt} \right) + \\ + \frac{1}{C} \cdot \left(-u_{c1} \cdot g_{11} + u_{c2} \cdot g_{12} + i_a \cdot k_1 - i_{c3} \right) \quad (18),$$

$$\frac{du_{c2}}{dt} = R_c \cdot \left(\frac{du_{c1}}{dt} \cdot g_{21} - \frac{du_{c2}}{dt} \cdot g_{22} + \frac{di_a}{dt} \cdot k_2 - \frac{di_{c4}}{dt} \right) + \\ + \frac{1}{C} \cdot \left(u_{c1} \cdot g_{21} - u_{c2} \cdot g_{22} + i_a \cdot k_2 - i_{c4} \right) \quad (19).$$

The time derivative of the flux linkages is divided into the transformer and speed EMF (10):

$$\frac{d[\psi]}{dt} = \frac{d[\psi]}{di} \frac{di}{dt} + \frac{d[\psi]}{d\varphi} \frac{d\varphi}{dt} \quad (20).$$

The values of incremental inductances /5/, which are the derivatives of flux linkages with respect to the current, and the values of the flux linkages at different angles and currents were obtained with the commercially available finite element method (FEM) program. Since we presume the speed of the motor to be constant, the following equation can be written (21):

$$\frac{d[\psi]}{dt} = [L] \frac{di}{dt} + \frac{d[\psi]}{d\varphi} \omega \quad (21).$$

By substituting the time derivative of the flux linkages in (1), (2) and (3) with (21) and by adding the time derivative of the capacitor voltages (18), (19), we get (22):

$$\begin{bmatrix} U \\ 0 \\ 0 \\ 0 \\ 0 \end{bmatrix} = \begin{bmatrix} R_{11} + R_2 & 0 & 0 & -1 & -1 \\ 0 & R_3 & 0 & -1 & 0 \\ 0 & 0 & R_4 & 0 & -1 \\ \frac{k_1}{C} & -\frac{1}{C} & 0 & -\frac{g_{11}}{C} & \frac{g_{12}}{C} \\ \frac{k_2}{C} & 0 & -\frac{1}{C} & \frac{g_{21}}{C} & -\frac{g_{22}}{C} \end{bmatrix} \cdot \begin{bmatrix} i_a \\ i_{c3} \\ i_{c4} \\ u_{c1} \\ u_{c2} \end{bmatrix} + \\ + \begin{bmatrix} L_{aa} & L_{a3} & L_{a4} & 0 & 0 \\ L_{a3} & L_{33} & L_{34} & 0 & 0 \\ L_{a4} & L_{34} & L_{44} & 0 & 0 \\ R_c \cdot k_1 & -R_c & 0 & -R_c \cdot g_{11} - 1 & R_c \cdot g_{12} \\ R_c \cdot k_2 & 0 & -R_c & R_c \cdot g_{21} & -R_c \cdot g_{22} - 1 \end{bmatrix} \cdot \\ \begin{bmatrix} \frac{di_a}{dt} \\ \frac{di_{c3}}{dt} \\ \frac{di_{c4}}{dt} \\ \frac{du_{c1}}{dt} \\ \frac{du_{c2}}{dt} \end{bmatrix} + \begin{bmatrix} \frac{d\psi_a}{dt} \\ \frac{d\psi_3}{dt} \\ \frac{d\psi_4}{dt} \\ 0 \\ 0 \end{bmatrix} \cdot \omega \quad (22).$$

Rearranging (22), we obtain the following equation:

$$\begin{bmatrix} \frac{di_a}{dt} \\ \frac{di_{c3}}{dt} \\ \frac{di_{c4}}{dt} \\ \frac{du_{c1}}{dt} \\ \frac{du_{c2}}{dt} \end{bmatrix} = \begin{bmatrix} L_{aa} & L_{a3} & L_{a4} & 0 & 0 \\ L_{a3} & L_{33} & L_{34} & 0 & 0 \\ L_{a4} & L_{34} & L_{44} & 0 & 0 \\ R_c \cdot k_1 & -R_c & 0 & -R_c \cdot g_{11} - 1 & R_c \cdot g_{12} \\ R_c \cdot k_2 & 0 & -R_c & R_c \cdot g_{21} & -R_c \cdot g_{22} - 1 \end{bmatrix}^{-1} \\ \cdot \left(\begin{bmatrix} R_{11} + R_2 & 0 & 0 & -1 & -1 \\ 0 & R_3 & 0 & -1 & 0 \\ 0 & 0 & R_4 & 0 & -1 \\ \frac{k_1}{C} & -\frac{1}{C} & 0 & -\frac{g_{11}}{C} & \frac{g_{12}}{C} \\ \frac{k_2}{C} & 0 & -\frac{1}{C} & \frac{g_{21}}{C} & -\frac{g_{22}}{C} \end{bmatrix} \cdot \begin{bmatrix} i_a \\ i_{c3} \\ i_{c4} \\ u_{c1} \\ u_{c2} \end{bmatrix} + \begin{bmatrix} U - \frac{d\psi_a}{dt} \cdot \omega \\ -\frac{d\psi_3}{dt} \cdot \omega \\ -\frac{d\psi_4}{dt} \cdot \omega \\ 0 \\ 0 \end{bmatrix} \right) \quad (23).$$

Eq. (23) represents the model of the system in the standard form of the state space formulation. At each time step the values of the inductances, the resistances and the flux linkages derivatives with respect to the angle are updated according to the angle (brush position) and main current i_a. Since the flux linkages, but not their derivatives, were obtained with FEM, the table of the flux linkages derivatives with respect to the angle were calculated from the table of the flux linkages before the solution to the system (23) was initiated. The system is solved by time stepping numerical integration.

3. FEM computed inductances and flux linkages and their dependence on the commutation

A large number of the finite element magnetostatic iterations had to be calculated to obtain the complete incremental inductance matrix and the flux linkage vector, since they depend on the current and the angle. They must be calculated at each angle and current step throughout all the currents values involved.

The inductance computation method used by the commercially available FEM program /7/ is based on Gyimesi and Ostergaard /8/. The method uses incremental energy, which is calculated around the working point, when the currents are incremented.

In Eq. (23) there are three currents; main current i_a, and two commutating currents, i_{c3} and i_{c4}. The inductance matrix and the flux linkage vector are dependent on all the three currents. The FEM magnetostatic solution should be calculated at each combination of these currents, which leads to an unmanageable number of calculations. Jet, since main current i_a has the greatest influence on iron saturation, it is presumed that commutation currents do not considerably change the inductance values. A number

of test calculations was made, using the following two commutation current forms:

1. *the linear commutation,* using the linear commutation current from $-i_a$ to i_a and the length of the commutation equals to the whole brush width;
2. *the 50% overcompensated linear commutation*, using also the linear commutation current from $-i_a$ to i_a but shortening the length of the commutation by 50%.

The results of these calculations with respect to the angle and at an unchanged value of the main current can be seen in Fig. 4. The maximum difference between the inductances is 5%, which is considered acceptable for further use. The difference is due to the slightly lower saturation at 50% overcompensated linear commutation.
A database table is created at each angle and current step. It consists of an inductance matrix and flux linkage entries. As the integration of Eq. (23) is progressing, the values in the table are interpolated from the nearest values of angles and currents in the table.

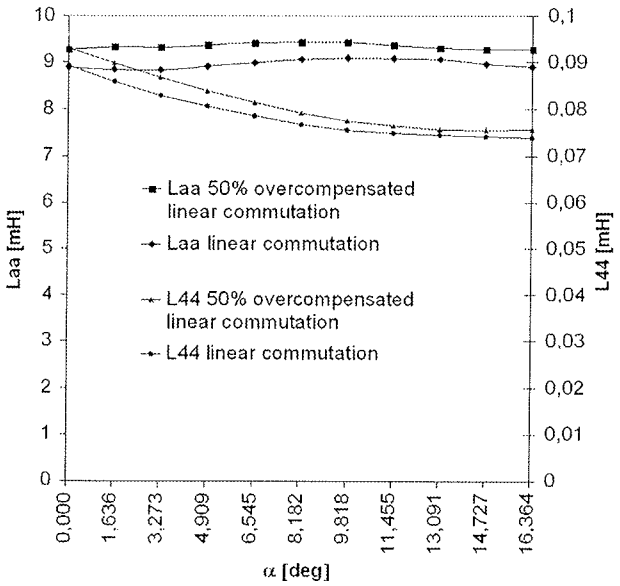

Figure 4: The inductance comparison at i_a=5A and at two different commutation forms - at 50% overcompensated linear commutation and at linear commutation.

4. The distributed brush resistance matrix, the brush-commutator contact resistances and the arc model

4.1. The distributed brush resistances

The internal brush resistances were calculated by the commercially available FEM package. These resistances are dependent on the brush to the commutator position. They were calculated according to /4/, where the cross-section of the brush is covered with an FE mesh. The result of the FEM computation is the voltage distribution throughout the cross-section of the brush, and the electric current density is calculated from this voltage distribution. On the side of the brush, where it touches the commutator bars, voltages are applied (Dirichlet boundary condition), depending on the brush to commutator position. On the opposite side, the end surface voltage is defined as zero. The brush FE mesh is shown in Fig. 5.

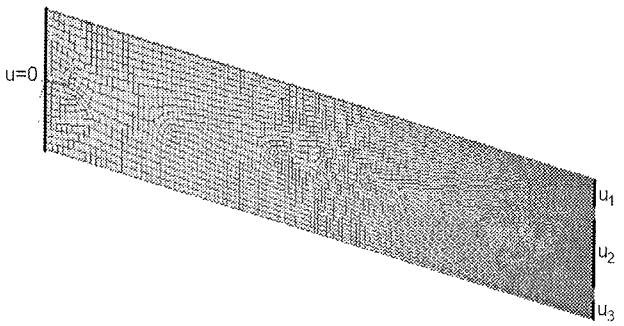

Figure 5: The brush FE model with the mesh and the boundary conditions.

The entries of the brush resistance matrix were calculated from the system energy /4/. Results dependent on the brush position are given in Fig. 6.

The initial commutator position is the position where the commutator groove is at the centre of the brush (α=0). At that position the brush covers two commutator bars and the brush matrix entries r_{33}, r_{13} and r_{23} are there infinite. The infinite values are replaced with high resistance values. From α=3.304° to 13.059° the brush covers three bars entirely, so each matrix entry is finite. Where the angle is larger than 13.059°, the brush again covers only two bars and the infinite resistance matrix entries are again replaced with high but finite values.

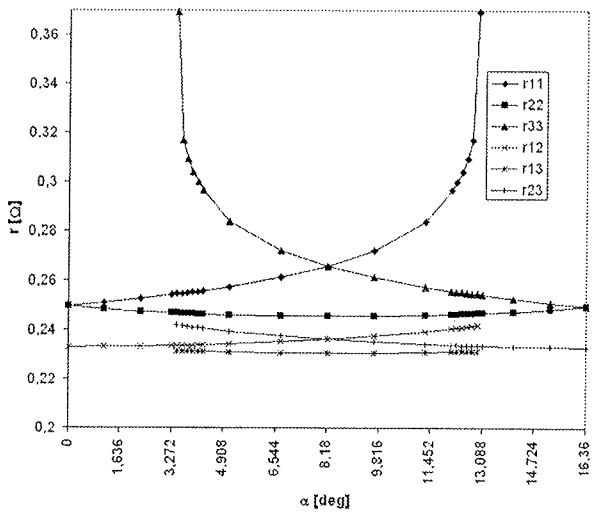

Figure 6: The FEM calculated brush resistance matrix entries

4.2. The brush-commutator contact resistances

The full brush contact resistance R_{full} is calculated from the average contact voltage drop and from the current at which the collector film is formed. The brush contact resistance due to the commutator position is calculated using the following equation:

$$r_c = R_{full} \cdot \left(A_{full} / A(\alpha)\right)^{0.75} \qquad (24).$$

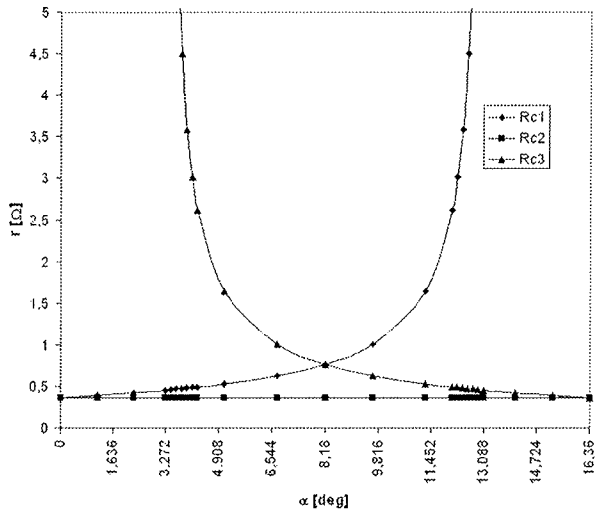

Figure 7: The brush – commutator bars contact resistances.

Here A_{full} represents the full commutator bar-brush contact area and $A(\alpha)$ commutator bar-brush contact area on instantaneous commutator position. The contact resistance equations are written for all the three commutator bars with regard the commutator position. At the initial and final commutator positions, two bars only are covered by the brush and one contact resistance has an infinite value replaced by a large finite value. The calculated resistances are shown in Fig. 7.

4.3. The arc model

When the commutator bar is leaving the brush, the conducting area $A=A_1$ draws near to zero and the contact resistance becomes infinite. The current density increases and causes vaporization of the surface material and formation of the electric arc. The conditions for the arc formation were thoroughly examined by Holm et al/9/ who measured U-I characteristics of the arc. The voltage at which the arc is formed (U_m) depends on the cathode material of the separating contacts, whereas the current at which the arc extinguishes (I_m) at the latest depends on the anode material. According to /9/, different authors have measured different values of I_m and U_m. In Table 1 these values for carbon and copper can be seen.

In our case, the source voltage is the AC voltage. So in one brush-commutator bar contact the cathode in one half of the AC cycle is copper and in the other half is carbon. At the other brush-commutator bar contact this is just the opposite. Average value for U_m and I_m, measured by Holm, are then used. They are 16.5V and 0.22A, respectively. These values were confirmed by our measurements on a motor equipped with an additional brush, closely following one of the main brushes. The voltage was measured over both brushes.

In the system described by Eq. (23), the arc characteristic is implemented by changing the value of R_{c1}, that is the contact resistance of the first commutator bar and the brush. When the contact voltage on the trailing edge of the brush reaches U_m, the arc is assumed to ignite and an apparent contact resistance is calculated by maintaining the arc voltage drop. This model is valid as long as the commutator bar is under the brush and the distance between them is constant. This distance is the thickness of the commutator film and other deposits. When the commutator bar leaves the brush, the contact voltage is no longer constant. It increases with the distance from the commutator bar. In this case, the arc U/I characteristic from /9/ is applied. The arc extinguishes when the arc current falls below a certain value derived from the U/I characteristics of the arc and of the load. The minimal arc current is larger than I_m. In our case this is 0.22A.

Under normal operating conditions of the universal motor, arcs under the brush appear very often. They affect the brush visibly; a blackened charred layer or a belt develops on the brush. A photography of such layer is shown in Fig. 8.

The contact resistance of the charred layer is about fifty times larger than the normal brush-bar contact resistance. This contact resistance is of no importance if the arc has already been ignited. It is important for the formation of the arc. If the charred layer is already formed, the contact resistance reaches the value at which, as a result of other conditions, the arc occurs. This happens at a lower angle compared to the clean brush. This means that the charred layer itself grows in the direction opposite to rotation. The growing of the charred layer stops when the system reaches equilibrium.

Table 1: I_m and U_m for carbon and copper, measured by different authors

	I_m [A]			U_m [V]			
Material	Ives	Fink	Holm	Ives	Gaulrapp	Fink	Holm
C	0.02		0.01	15.5			20
Cu		1.15	0.43		12.5	8.5	13

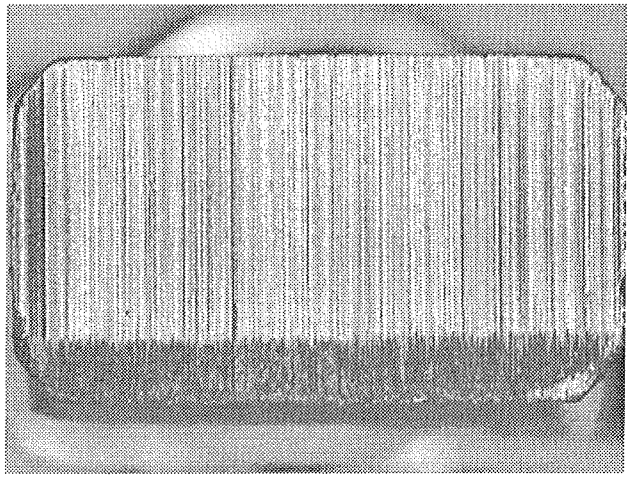

Figure 8: Photography of a brush with a charred layer.

In the model, instead of one contact resistance R_{c1} we have two contact resistances, i. e. the resistance of the clean brush and the resistance of the charred layer with a variable width as it is depicted on Fig. 9.

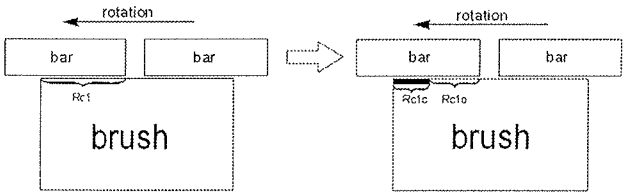

Figure 9: Change in the contact resistance Rc1 due to the charred layer on the brush.

Fig. 10 shows the contact resistance R_{c1} which includes the increased resistance of the charred layer.

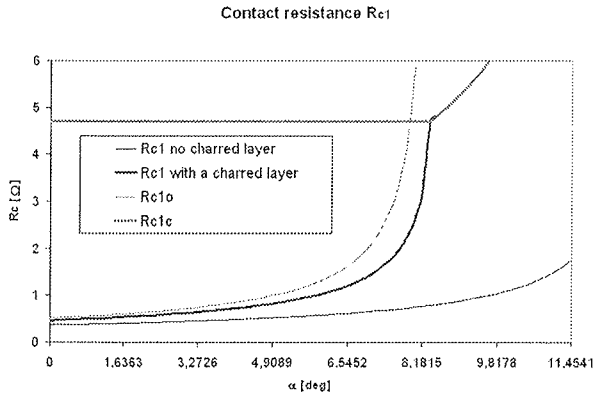

Figure 10: The comparison of R_{c1} with and without the charred layer.

5. Solving the system of equations

The Runge-Kutta method of the fourth order was used for solving the system of equations (23). To solve the system, we need initial values for the system variables i_a, i_{c3}, i_{c4}, u_{c1} and u_{c2}. The initial values for these variables were set to zero. The system (23) was now solved. If conditions for the arc formation developed, the arc model is applied. The starting position of the commutator ($\alpha = 0°$) is at the position where the commutator groove is aligned with the center of the brush. The ending position ($\alpha = \alpha_p = 360°/22 = 16.36°$ if there are 22 commutator bars) is defined by the position, at which the next commutator groove is aligned with the center of the brush. The values of the system variables at the ending position of the commutator are used for the initial conditions for the next iteration in a way as it is shown in Eq. (25):

$$\begin{aligned} i_{a,i+1}(\alpha = 0°) &= i_{a,i}(\alpha = \alpha_p) \\ i_{c3,i+1}(\alpha = 0°) &= i_{c4,i}(\alpha = \alpha_p) \\ i_{c4,i+1}(\alpha = 0°) &= i_{a,i}(\alpha = \alpha_p) \\ u_{c1,i+1}(\alpha = 0°) &= u_{c2,i}(\alpha = \alpha_p) \\ u_{c2,i+1}(\alpha = 0°) &= R_4 \cdot i_{a,i}(\alpha = \alpha_p) + \frac{d\psi_{4,i}(\alpha = \alpha_p)}{dt} \end{aligned} \quad (25),$$

where i is the index of the current iteration.

In the case of the DC source voltage, the system iterates until the values of the system variables at the end of the iteration are the same as the values of the system variables from the previous iteration within the tolerance limits. If an arc develops in any of the iterations, the width of the charred layer is calculated and then used for the next iteration. The system usually reaches the converged value in less than 100 iterations.

In the case of the AC source voltage, the solution to the system is much more time consuming. At 30000 rpm, the motor makes 10 revolutions in one 50Hz AC cycle. This means 220 iterations in one AC cycle for the commutator with 22 segments. At each commutation iteration the width of the charred layer is remembered and at the end of one AC cycle the average width of the charred layer is calculated and used for the next AC cycle. The iteration stops when the RMS current and the charred layer width stop changing. This is usually after several tens of AC cycles.

6. The simulation and the verification results using the commutator without the integrated capacitors

At the first the simulation was done for the case without the capacitors. Since the capacitors are already integrated in the numerical model, the capacitors are presumed to have no effect on commutation, if a large value of resistance R_c is chosen.

The simulated and the measured data were based on the technical data for a vacuum cleaner motor, equipped with 22 commutator bars and 22 slots. It is a standard two-pole universal motor having an effective brush advance angle

of 24.5°. The value of the main current was 3.6A and the motor speed was 22000 rpm. This is below the nominal working point of the motor, because our test motor did not allow higher speed and current. The nominal voltage of the analysed unit is 230V, but the voltage of 180V was used in our tests.

The measurements were made on a special test motor, which has two rotor coils connected to the slip rings through a hollow shaft. The brushes on the slip rings are special low resistance brushes, made of graphite with large portion of copper. On these brushes it is possible to measure the commutation current. On the Fig. 11, a photography of the test motor with slip rings is shown.

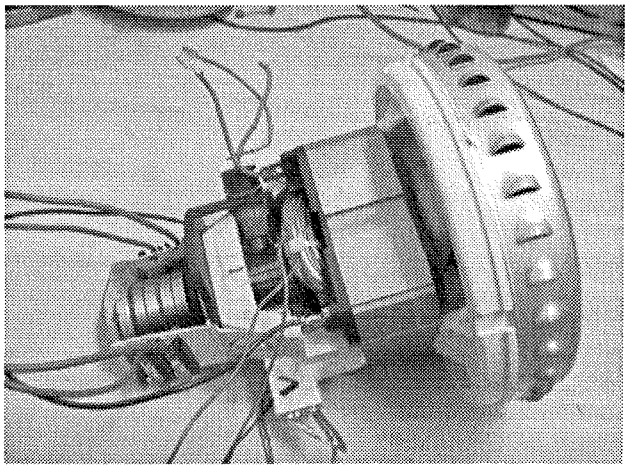

Figure 11: The test motor with the slip rings.

The five important positions of the commutator were defined, as it is shown in Fig. 12.

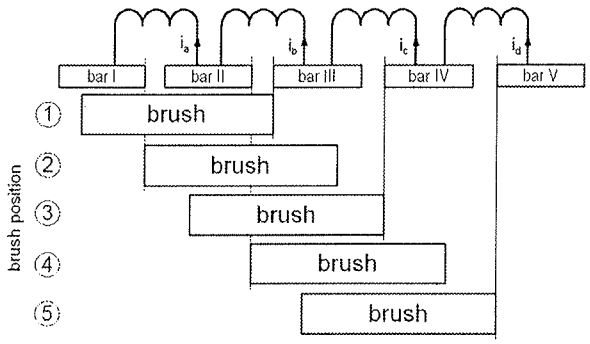

Figure 12: The five important commutator positions.

Fig. 13 shows the simulated commutating current. The charred layer width was calculated to be 1°. This is the width of 0.2mm on the brush. This means there was the arc under the brush with the constant voltage. The current fell below I_m when the commutator bar left the brush, so there was no arc in the air gap between the trailing edge of the brush and the leaving bar. In Fig. 13, two identical sequential calculations are shown thus presenting one complete commutation (current I_b).

In some commutator positions, two sequential coils commutate and affect each other. For example, when the bar III enters the brush, the direction of the current I_a changes. It begins to decrease despite having no direct contact with the bar III. This happens because of the mutual inductance of the coils a and b. The opposite happens when the bar I enters the charred layer; the arc develops and rapidly changes I_a and also I_b - the commutation of I_b is slowed down. It is seen, that the commutation of one coil current worsens the commutation of the other. But if the arc develops, the other coil dissipates the energy of the arc because of the mutual inductance between these coils. As the arc develops in the charred layer, the arc current decreases quickly. When it drops bellow the limit value, the arc extinguishes. In our case this happened just before the bar II left the brush.

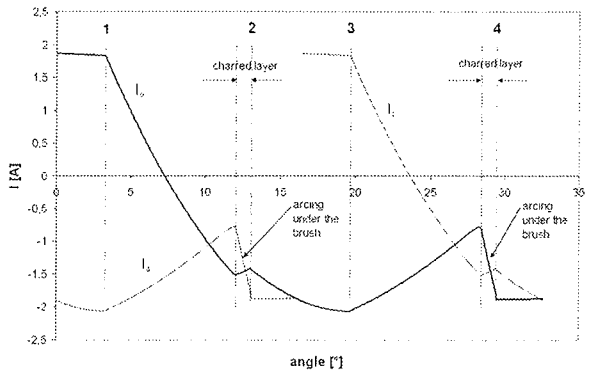

Figure 13: The simulated commutation currents without the capacitors.

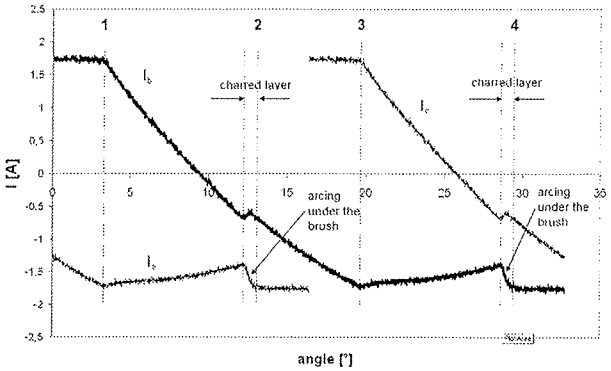

Figure 14: The measured commutation currents without the capacitors.

Let us now examine the comparable measurements. The measurements results are shown in Fig. 14. The measured commutating current has the same form as the calculated one. At the beginning of the commutation of the current I_b - the point 1 - the simulated current commutated faster than the measured current. The effect of arcing of the previous current can clearly be seen on the simulated and on the measured current. The largest difference between these two currents happens from the points 3 and

4, where the next current I_c starts to commutate. The current I_b at simulation starts to increase rapidly, at measurement this increase of the current is not so steep. The current difference, which dissipates the energy through arcing is therefore larger at simulation. The length of the charred layer is 0.8° in both cases.

It is clearly shown, that arcing under the brush did occur, when a commutator without integrated capacitors was used.

7. The simulation and the verification results using the commutator with the integrated capacitors

The integration of the capacitors in the commutator is seen in Fig. 15. The multilayer ceramic capacitors, manufactured as surface mounted chips, were used. The dimensions of capacitors were 2.0x1.25x1.2mm. The cross-section of such capacitor is seen in Fig. 16. The ceramic dielectric used was the stable 2R1. This material is made of ceramic materials, which are ferroelectric, principally barium titanate. The capacitors of the ferroelectric types have a nonlinear temperature characteristics, the capacitance and tand are effected by temperature, voltage and frequency. The material 2R1 was used because it has the best compromise between capacitance per volume unit and temperature and voltage stability. There is not much space in the commutator, so the size of the capacitor is critical. The above mentioned dimensions are maximal, which can be used in the given commutator. The maximal capacitance of capacitor with dimensions 2.0x1.25x1.2mm, using the 2R1 dielectric, is 1μF and its withstand voltage is 100V.

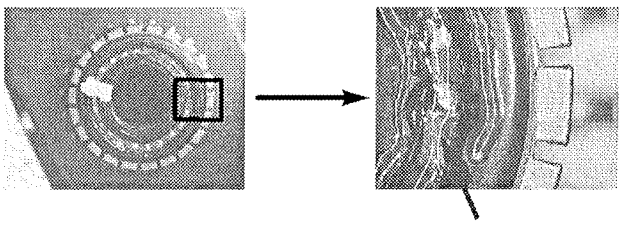

Figure 15: The integration of the capacitors in the commutator.

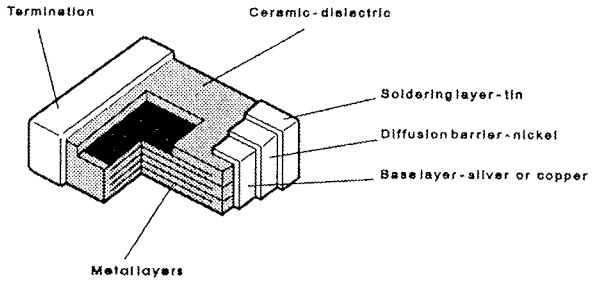

Figure 16: The cross-section of the used ceramic capacitors.

The capacitors were integrated into the commutator because of large centrifugal forces which are present at the rotational speed up to 50,000 rpm. As it is seen in Fig. 15, the capacitors were firmly soldered into the circular groove at the top of the commutator. The groove was then filled with a clear plastic glue, which further fixed the capacitors into the groove and also prevented any debris from the brush to make any additional unwanted contacts.

The capacitors in the commutator work in a very harsh environment. As it was stated above, it is exposed to large centrifugal forces. The temperatures on the commutator surface reach the values of 110°C - 120°C. On the inside of the commutator the temperatures are lower by 10°C - 20°C. So the ceramic material must not loose its dielectric capability because of temperatures around 100°C.

The voltage of the capacitor must not exceed the nominal voltage of the capacitor, and it also must not reach too high value to cause additional arcing. The theoretical maximal capacitor voltage can be estimated using the magnetic and electrical energy equations. In Eq. (16) it is presumed, that all the magnetic energy, stored in the commutating winding at the angle, where the commutator bar leaves the brush, changes into the electrical energy of the capacitor.

$$\frac{L_{33}\cdot(\Delta i)^2}{2}=\frac{C\cdot(U_{C\max})^2}{2} \qquad (26),$$

where:

Δi = 1A	the current difference,
$U_{C\max}$ = 16,5V	maximal allowed capacitor voltage to avoid arcing,
L_{33} = 240 μH	inductance of the commutating winding.

The value of the required capacitance can be calculated using the Eq. (27), which is derived form (26):

$$C=L_{33}\cdot\left(\frac{\Delta i}{U_{C\max}}\right)^2=918\,\mathrm{nF} \qquad (27).$$

With this capacitance the capacitor voltage will not exceed the arcing limit U_m=16,5V at the given working point. It must be emphasized, that the inductance L_{33} is dependent both on the main current and on the angle of rotation - this mean the position of the rotor. The current difference Δi depends on the behavior of the whole system. So this calculation is valid only for the estimation of the required capacitance for the working point.

The capacitors which were used in the simulation and in the measurement had the capacitance C= 1μF, which leaves us slight safety margin. The capacitors nominal voltage is 100V.

The simulation results are seen in Fig. 17. To avoid confusion only one commutating current is shown. The current has first oscillation at the position 2, which is the conse-

quence of the previous commutation. From the position 3 to 4 the current starts to increase, because at the position 3 the next winding starts to commutate. The same effect can be seen in Fig. 13, where the commutation without capacitors is shown. When the commutator bar reaches the end of the brush at the position 4, the current starts to flow into the capacitor. This is the beginning of LC oscillations, which are damped because of the winding resistance R_3 and because of the damping resistance R_c. At the angle 45°, the oscillations have not yet ceased.

In Fig. 18 the simulated capacitor voltage is shown. Only the second part of the simulation is shown - the rotor positions 3, 4 and 5. At the position 4 the commutator bar is leaving the brush and at that angle the energy starts to flow from inductance into capacitor. Therefore the capacitor voltage increases. The maximal capacitor voltage reaches the value of 17V, which is slightly above the estimated value. But this voltage is can cause arcs, if it is present at position 4, where the commutator bar is still close to the brush. When the bar - brush distance increases, the voltage, necessary for arcing, increases as well. At the angle 32°, where the capacitor voltage is maximal, the distance of the brush from the bar is 3°, which is 0,65mm. According to /10/ at that distance the required arcing voltage is around 35V. The capacitor voltage has not reached this value at which arcing could occur. So the rightly chosen capacitors prevent arcing.

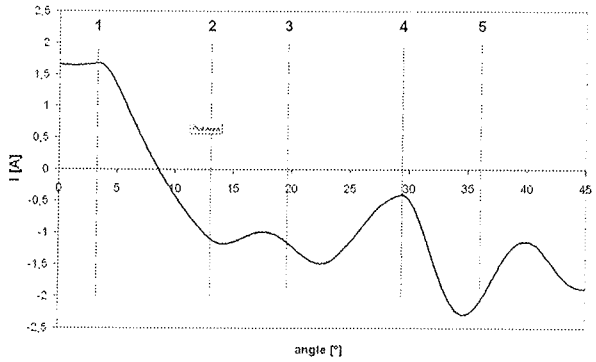

Figure 17: The simulated commutation currents with the integrated capacitors C=1μF.

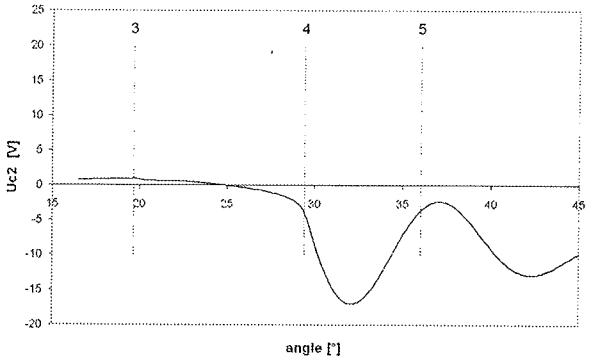

Figure 18: The simulated capacitor voltage.

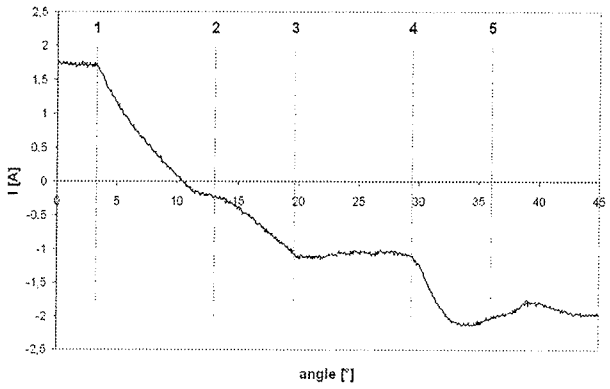

Figure 19: The measured commutation currents with the integrated capacitors C=1μF.

The measurements were made on another test motor with the same construction as in Fig. 11, but with capacitors integrated in the commutator. The measured results are in Fig. 19. The current difference at the position 4, where the commutator bar is leaving the brush, is smaller than in the simulation, so the oscillation afterwards have smaller amplitude. The oscillation at the position 2 are smaller as well. This is because the commutation of the previous coil has smaller oscillations and the effect on the observed commutation also diminishes. Measurements show that there is no arcing.

Quality of the commutation has direct effect on the lifetime of the universal motor. Arcing causes migration of material on the brush-commutator contact, specially the brush material. The brush material losses are divided to loses due to the mechanical causes- friction and vibration - and to the losses due to electrical one - arcing. It was proven in this work, that to prevent arcing the integrated capacitors have to be used. Because of that, the tested actual lifetime of the motors with integrated capacitors increases by 25% to 30%.

5. Conclusions

The method for the analysis of the commutation current and arcing of the high-speed universal motor with the integrated capacitors built in the commutator is presented in this paper. The analysis is done by the mathematical model. The model consists of the circuit elements obtained with the finite element method. These elements are inductances, flux linkages and internal brush resistances. The actual brush - commutator segment overlapping of 1.8 is used. The contact resistances are thoroughly examined and the arc model is implemented. The effect of the charred layer on the brush is considered as the increased contact resistance. The charred layer is caused by the arc under the brush. As the charred layer contact resistance is very high, it actually helps commutation. Because of this layer the commutation ends before the commutator bar leaves the brush and no arc develops in the air gap at the trailing edge of the brush. But still, there is the arc under the brush,

and the brush wears down more rapidly than it would in absence of the arc.

The method for the estimation of the required integrated capacitance is presented too. The criterion for the capacitance choice was the capacitor voltage which must not exceed the value, at which arc is formed.

The commutation currents with and without the capacitors are compared. It is shown, that without the capacitors arcing under the brush occurs. When capacitors are added to the commutation circuit, no more arcs occur, and the lifetime of the motor is extended by 25-30%.

The calculated commutation currents are also compared with the measured ones. The measurements were made on special test motors with the slip rings. The results of the calculation are found satisfactory.

With the appropriate machinery the integration of capacitors into the commutator is possible in the serial production. The cost of such an enhanced commutator in not too high and it is estimated that for high performance universal motors that kind of commutator is going to be used.

6. References

/1/ J. S. Ewing, B. R. Patel: *Contribution to Commutation Analysis*. IEEE Power Engineering Society Winter Meeting, New York, January 1972, pp1663-1668.

/2/ R. Schröder, K. Oberretl: *Neues Verfahren zur Berechnung der Kommutierung von Gleichstrommaschinen unter Berücksichtigung der Bürstenübergangswiderstände*. Archiv für Electrotechnik, No.73, Springer Verlag 1990, 69-79

/3/ T. Matsuda, T. Moriyama, N. Konda, Y. Suzuki, Y. Hashimoto: *Method for Analysing the Commutation in Small Universal Motors*. IEE Proc.-Electr. Power Appl., Vol. 142, No. 2, March 1995

/4/ R. H. Wang, R. T. Walter: *Modeling of Universal Motor Performance and Brush Commutation Using Finite Element Computed Inductance and Resistance Matrices*. IEEE Trans. On Energy Converion, vol. 15, No.3, september 2000

/5/ R. H. Wang, R. T. Walter: *Computer Aided Simulation of Performance and Brush Commutation for Universal Motor with Two Coils per Armature Slot*. Intern. Conf. On Electric Machines and Drives IEMD '99

/6/ T. W. Nehl, F. A. Fouad, N. A. Demerdash: *Determination of Saturated Values of Rotating Machinery Incremental and Apparent Inductances by an Energy Perturbation Method*. IEEE Trans. On Power Apparatus and Systems, vol. PAS-101, No.12, December 1982

/7/ Erle I. Shobert, II: *Carbon Brushes*, Chemical Publishing Company, Inc., New York, 1965

/8/ Ansys 6.0: *ANSYS, Inc. Theory Reference*, 2001

/9/ Gyimesi, Miklos and Ostergaard, Dale: *Inductance Computation by Incremental Finite Element Analysis*, CEFC 98, Tucson, Arizona (1998)

/10/ R. Holm: *Electric Contacts, Theory and Application*, 4th Edition, Springer Verlag, Berlin/Heidelberg/New York (1979)

/11/ F. Pavlovčič, J. Nastran: *Reducing EMI of commutator motors by optimizing brush-to-segment width ratio*. Inf. MIDEM, 2002, Vol.32, No.3, pp. 189-193.

Boris Benedičič, M.Sc.
R&D Department
Domel d.d.
Otoki 21, 4228 Železniki
boris.benedicic@domel.si

Dr. France Pavlovčič
Environmental Agency of the Republic of Slovenia
Ministry of environment, spatial planning and energy
Vojkova 1b, 1000 Ljubljana
france.pavlovcic@gov.si

Prof. dr. Janez Nastran
Faculty for Electrical Engineering
University in Ljubljana
Tržaška 25, 1001 Ljubljana
janez.nastran@fe.uni-lj.si

Jožica Rejec, M.Sc.
R&D Department
Domel d.d.
Otoki 21, 4228 Železniki
boris.benedicic@domel.si

Prispelo (Arrived): 31.10.2003 *Sprejeto (Accepted): 25.02.2004*